Electrodeposition of simonkolleite as a low-temperature route to crystalline ZnO films for dye-sensitized solar cells

Esdras Canto-Aguilar, Carlos González-Flores, Diecenia Peralta-Domínguez, José Andres-Castán, Renaud Demadrille, Manuel Rodríguez-Pérez, Gerko Oskam

▶ **To cite this version:**

Esdras Canto-Aguilar, Carlos González-Flores, Diecenia Peralta-Domínguez, José Andres-Castán, Renaud Demadrille, et al.. Electrodeposition of simonkolleite as a low-temperature route to crystalline ZnO films for dye-sensitized solar cells. Journal of The Electrochemical Society, 2022, 169 (4), pp.042504. 10.1149/1945-7111/ac62c8 . hal-03636172

HAL Id: hal-03636172
https://hal.science/hal-03636172

Submitted on 22 Jan 2024

HAL is a multi-disciplinary open access archive for the deposit and dissemination of scientific research documents, whether they are published or not. The documents may come from teaching and research institutions in France or abroad, or from public or private research centers.

L'archive ouverte pluridisciplinaire **HAL**, est destinée au dépôt et à la diffusion de documents scientifiques de niveau recherche, publiés ou non, émanant des établissements d'enseignement et de recherche français ou étrangers, des laboratoires publics ou privés.

Distributed under a Creative Commons Attribution 4.0 International License

Journal of The Electrochemical Society

The Electrochemical Society
Advancing solid state & electrochemical science & technology

OPEN ACCESS

Electrodeposition of Simonkolleite as a Low-Temperature Route to Crystalline ZnO Films for Dye-Sensitized Solar Cells

To cite this article: Esdras J. Canto-Aguilar *et al* 2022 *J. Electrochem. Soc.* **169** 042504

View the article online for updates and enhancements.

You may also like

- Enzyme-Catalyzed Oxygen Reduction Reaction in Biofuel Cells: Analytical Expressions for Chronoamperometric Current Densities
M. Rasi, L. Rajendran and M. V. Sangaranarayanan

- First-Principles Investigation of Electronic Structure and Energy Level Scheme of Phosphors: The Lanthanide-Doped $Sr_2P_2O_7$
Jinying Yu, Yufan Fan, Lina Wu et al.

- Tris(4,4-di-*t*-butyl-2,2-bipyridine)cobalt: Cation Effects on the Voltammetry at ITO and on Mediator Performance in Dye Sensitized Solar Cells
Di Xue, Lance N. Ashbrook, Ross S. Gaddie et al.

Measure the Electrode Expansion in the Nanometer Range.
Discover the new ECD-4-nano!

EL-CELL®
electrochemical test equipment

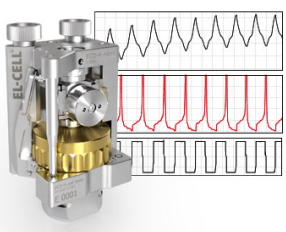

- Battery Test Cell for Dilatometric Analysis (Expansion of Electrodes)
- Capacitive Displacement Sensor (Range 250 µm, Resolution ≤ 5 nm)
- Detect Thickness Changes of the Individual Electrode or the Full Cell.

www.el-cell.com +49 40 79012-734 sales@el-cell.com

This content was downloaded from IP address 193.48.96.13 on 22/01/2024 at 09:17

Journal of The Electrochemical Society, 2022 **169** 042504

Electrodeposition of Simonkolleite as a Low-Temperature Route to Crystalline ZnO Films for Dye-Sensitized Solar Cells

Esdras J. Canto-Aguilar,[1,2,z] Carlos A. González-Flores,[2] Diecenia Peralta-Domínguez,[2] José M. Andres-Castán,[3] Renaud Demadrille,[3,z] Manuel Rodríguez-Pérez,[1] and Gerko Oskam[2,4,*,z]

[1]*Facultad de Ingeniería, Universidad Autónoma de Campeche-Campus V, San Francisco de Campeche, Campeche 24085, México*
[2]*Department of Applied Physics, CINVESTAV-IPN, Mérida, Yucatán 97310, México*
[3]*Université Grenoble Alpes, CEA, CNRS, IRIG-SyMMES, Grenoble 38000, France*
[4]*Department of Physical, Chemical and Natural Systems, Universidad Pablo de Olavide, Seville 41013, Spain*

A pulsed electrodeposition procedure has been developed to prepare macroporous films of the semiconducting mineral simonkolleite, $Zn_5(OH)_8Cl_2{\cdot}H_2O$, on glass/FTO substrates. The morphology is characterized by the presence of smooth, micron-sized hexagonal platelets, and relatively thick films of 6 μm can be prepared in about 15 min. Simonkolleite can be transformed into crystalline, mesoporous ZnO using a relatively low temperature thermal treatment (250 °C). While the macrostructure of hexagonal platelets is maintained, they become mesoporous due to the removal of water and Cl^--containing reaction products. Dye-sensitized solar cells were fabricated with both simonkolleite and ZnO films, using the recently reported fully organic benzothiadiazole-based photosensitizer MG-207, and an electrolyte solution based on either the I^-/I_3^- or the $Co(bpy)_3^{2+/3+}$ redox couple. An efficiency of 1.74% has been obtained for ZnO/MG-207/$Co(bpy)_3^{2+/3+}$ solar cells, illustrating the promise of crystalline, mesoporous ZnO obtained via a low-temperature simonkolleite route for portable and lightweight devices based on flexible substrates.

© 2022 The Author(s). Published on behalf of The Electrochemical Society by IOP Publishing Limited. This is an open access article distributed under the terms of the Creative Commons Attribution 4.0 License (CC BY, http://creativecommons.org/licenses/by/4.0/), which permits unrestricted reuse of the work in any medium, provided the original work is properly cited. [DOI: 10.1149/1945-7111/ac62c8]

Manuscript submitted February 4, 2022; revised manuscript received March 25, 2022. Published April 8, 2022.

Supplementary material for this article is available online

Electrodeposition is a widely used technique in industry, for example, in purification processes, selective extraction, protective coating application, metal finishing, ULSI metallization, and deposition of semiconducting materials.[1] The attraction of electrodeposition is largely related to the low-cost, simple processing and scalability of the method, as well as the precise control over the characteristics of the deposit through the electrochemical processing parameters such as plating bath composition, applied potential or current, temperature, etc. Electrodeposition can be categorized depending on the power supply source (potentiostatic or galvanostatic), mechanism (anodic or cathodic), cell configuration (2 or 3-electrode electrochemical cell) or by the kind of perturbation applied (constant or pulsed voltage/current). Each plating method offers specific advantages and its selection will depend on the desired characteristics in terms of composition, quality and deposition speed.[2,3]

The use of electrodeposition to synthesize semiconducting materials started decades ago with the deposition of II–VI materials such as CdS and CdTe, however, the continuous advance in the development of electronic devices has since then motivated intense research on other binary, ternary, and quaternary semiconductors including ZnTe, ZnO, $CuInSe_2$, Cu_2ZnSnS_4, $CuInGaSe_2$, etc.[4,5] The electrochemical synthesis of metal oxides is of great interest since many are semiconductors with band gap energies ranging from low values to several eV. This characteristic makes them suitable for a large variety of applications such as transparent conductive oxides, sensors, lasers, transistors, electrodes in electrochromic devices and dynamic windows[6,7] or electron transporting layers in photovoltaics, as is the case for ZnO.[5,8–10] Zinc oxide is an n-type semiconductor with direct band-to-band transitions and a relatively wide band gap of 3.3 eV, high exciton binding energy of 60 meV, excellent stability under high-energy radiation, and with superior electron transport properties compared to TiO_2.[11,12] An especially important characteristic of electrochemically synthesized ZnO is the possibility to obtain a variety of morphologies, ranging from quantum dots and nanostructures of any shape and form to films with either dense or open structures, depending on the bath composition, pH and temperature.[11,13–16] The attractive properties of ZnO make it an interesting material for application in photovoltaic systems, including in dye-sensitized solar cells.

In order to meet the increasing global energy demand, conversion of solar energy to either usable thermal, chemical or electrical energy is key to the sustainable development of present society.[17] The dye-sensitized solar cell (DSSC) is a third-generation system suitable for a variety of applications ranging from IoT (Internet-of-Things) devices to building-integrated photovoltaics (BIPV), combining the advantages of the use of abundant materials, mild processing conditions, and low-energy fabrication methods.[9,18–20] TiO_2 is generally the material of choice, however, both the synthesis of the TiO_2 nanomaterial and the fabrication of nanostructured, mesoporous film requires high temperatures up to 500 °C, which affects the cost analysis as well as its applicability in flexible and light-weight photovoltaics.[21–24] Electrodeposition represents a green chemistry solution with the ability to fabricate crystalline ZnO films at much lower processing temperatures.[25]

In this work, we present the electrodeposition of thick films of a zinc hydroxychloride material - the mineral simonkolleite—onto FTO, using a fast pulse plating method. Simonkolleite is a semiconductor that can be directly used in DSSCs, but can also be transformed in a highly porous and crystalline ZnO matrix with well-defined macrostructure after a relatively low-temperature thermal treatment at 250 °C. We illustrate the applicability of the electrodeposited ZnO film in a dye-sensitized solar cell using a fully organic dye not previously used for ZnO systems, and show that a $Co(bpy)_3$-based redox couple provides better performance than the traditional I^-/I_3^- couple. These characteristics open the possibility to the use of flexible substrates, such as flexible glass,[26] metallic foils[22] or high-temperature stability conductive polymers,[27] for the fabrication of portable and lightweight photovoltaic devices.

*Electrochemical Society Member.
[z]E-mail: esdras.canto@cinvestav.mx; esdrasreynolds@hotmail.com; gerko.oskam@cinvestav.mx

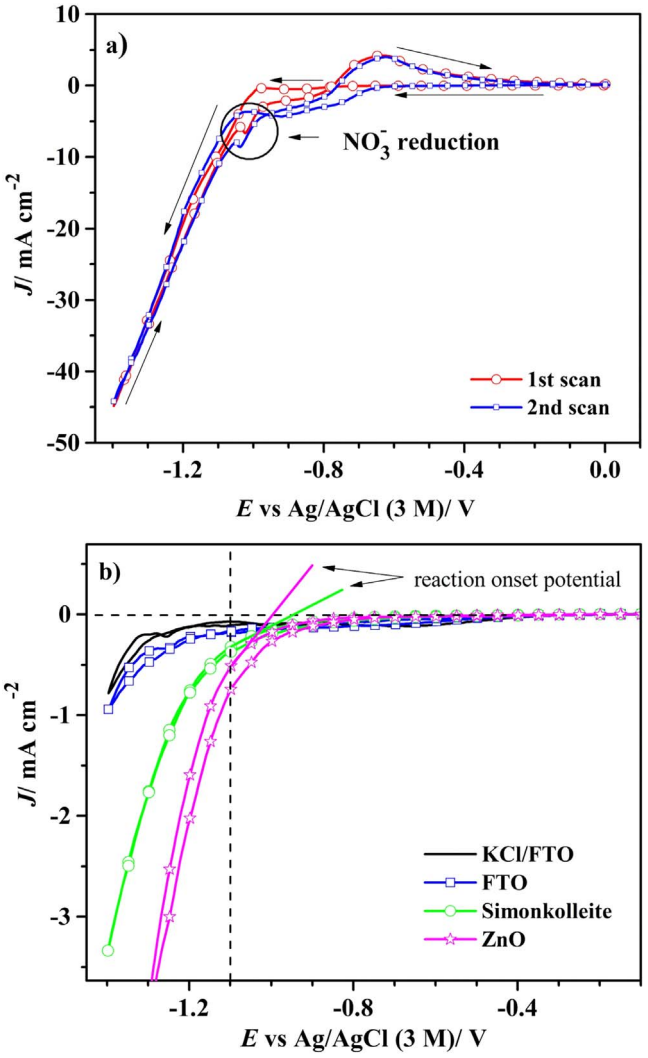

Figure 1. Cyclic voltammetry for electrolyte solutions purged with N_2 at pH 6 and at 70 °C, in the potential window from 0 to −1.4 V vs Ag/AgCl (3 M) and at a scan rate of 5 mV s^{-1}: (a) 0.1 M $Zn(NO_3)_2{\cdot}6H_2O$ + 0.1 M KCl aqueous solution at FTO; (b) 0.2 M $NaNO_3$ + 0.1 M KCl aqueous solution at different electrodes.

Experimental

The electrodeposition solutions used in this work have been electrochemically characterized by cyclic voltammetry (CV) with a Gamry potentiostat/galvanostat/ZRA 3000 employing a classic three-electrode system with Ag/AgCl (3 M KCl) as reference, a Pt counter electrode and a SnO_2:F-coated glass substrate (FTO, TEC 7 Ω sq^{-1}, Xop Glass) as working electrode. The working electrode was cleaned in an ultrasonic bath for 30 min in ethanol (J.T Baker, 99%), and sintered at 450° for 1 h as pretreatment. Porous films of Zn-containing materials onto FTO were obtained from a 0.1 M $Zn(NO_3)_2{\cdot}6H_2O$ (Sigma-Aldrich, ⩾99.0%) + 0.1 M KCl (Sigma-Aldrich, ⩾99.0%) aqueous solution at 70 °C and pH 6.0, using a galvanostatic pulsed method. For the deposits, a 0.5 cm^2 area was delimited with polyester tape (Cole-Parmer) and activated with 2 M H_2SO_4 (Sigma-Aldrich, 95.0%–98.0%), followed by rinsing with deionized water (18 MΩ cm). The same three-electrode cell configuration was used as previously described for the CV experiments. The Electrodeposition procedure was designed to increase the speed of NO_3^- reduction and achieve the formation of thin films in a fast and uniform manner. In particular, we used an elevated plating bath temperature of 70 °C and pulse plating; further details are provided in the corresponding sections in the results and discussion.

The crystal phase and composition of the materials deposited was analyzed with a Siemens D-5000 diffractometer (Cu-Ka radiation) operated at 34 kV and 25 mA; the diffraction patterns were collected from 5° to 70° (2θ) with a 0.02° step size, 2 s integration time, with the films at a 3° inclination. SEM images were taken using a scanning electron microscope (JEOL JSM 7600 F) operated at an accelerating voltage of 15 kV and using the in-lens (SEI) secondary electron detector. The UV/Vis diffuse reflectance characterization of the films deposited was carried out using a Thermo Scientific Evolution 220 UV–vis spectrometer equipped with an integrating sphere.

Dye-sensitized solar cells (DSSCs) were prepared with the electrodeposited films, both before and after a heat treatment as specified in the respective sections in the results and discussion. The dye used in this work was the organic benzothiadiazole-based MG-207 dye, which was recently reported and characterized in TiO_2-based DSSCs.[28] After a heat pretreatment, the working electrodes were immersed in a 0.2 mM MG-207 sensitizing solution with 2 mM chenodeoxycholic acid (CDCA; Sigma-Aldrich, ⩾97%) as coadsorbent in a mixture of chloroform (Sigma-Aldrich, ⩾99.5%) and ethanol (Sigma-Aldrich, ⩾99.5%) (1:1 v/v). The films were removed from the dye solution after 3 h and carefully washed with the same mixture of chloroform/ethanol. The sensitized working electrode and a FTO counter electrode with a thin Pt coating, obtained by spreading a drop of Platisol T (Solaronix) on the conductive side of the electrode and subsequent heating at 450 °C for 5 min, were sealed in a sandwich configuration using a Surlyn (50 μm, Dyesol) separator by heating at 210 °C for 2.5 min. An electrolyte solution consisting of 0.05 M I_2 (Sigma-Aldrich, ⩾99.8%), 0.2 M 4-tert-butylpyridine (TBP, Sigma-Aldrich, 98%), and 0.27 M 1,2-dimethyl-3- propylimidazolium iodide (DMPII, Solaronix, ⩾98%) in CH_3CN (Sigma-Aldrich, 99.8%) or 0.22 M $[Co(2,2'\text{-bpy})_3][B(CN)_4]_2$ (Eversolar, 98%), 0.05 M $[Co(2,2'\text{-bpy})_3][B(CN)_4]_3$ (Dyenamo), 0.1 M $LiClO_4$ (Sigma-Aldrich, ⩾95%) and 0.2 M TBP in CH_3CN was introduced inside the cell through a pair of holes previously perforated in the counter electrode, and the solar cell was subsequently sealed with Surlyn and a microscope cover glass, pressed under heating.

Photovoltaic characterization was performed using a set-up consisting of a 450 W ozone-free Xe-lamp (Newport Corporation) with a 10 cm water filter and an Air Mass 1.5 Global (AM 1.5 G) optical filter (Newport Corp.), calibrated to an irradiance of 100 mW cm^{-2} on the surface of the solar cell using a certified 4 cm^2 monocrystalline silicon reference cell with incorporated the KG-5 filter. Current density - voltage curves (J–V) were recorded with an Autolab PGSTAT302N/FRA2 (Metrohm Autolab).

Results and Discussion

Electrodeposition of simonkolleite and conversion to ZnO.— The indirect electrodeposition of metal oxides using NO_3^- as an oxidizing agent is a well-known method to deposit thin films with controlled morphology and thickness. For the electrodeposition of ZnO from nitrate solutions, a series of well-defined reactions have been proposed, which lead to the condensation of amorphous $Zn(OH)_2$ and the subsequent formation of crystalline ZnO films on the working electrode:[25,29–34]

$$NO_3^-(aq) + H_2O(l) + 2e^- \rightarrow NO_2^-(aq) + 2\ OH^-(aq) \quad [1]$$

$$2\ H_2O(l) + 2e^- \rightarrow H_2(g) + 2\ OH^-(aq) \quad [2]$$

$$Zn^{2+}(aq) + 2\ OH^-(aq) \rightarrow Zn(OH)_2(s) \quad [3]$$

$$Zn(OH)_2(s) \rightarrow ZnO\ (s) + H_2O\ (l) \quad [4]$$

The reduction of NO_3^- (Eq. 1) results in the generation of surface OH^-, which leads to a local pH increase and subsequent

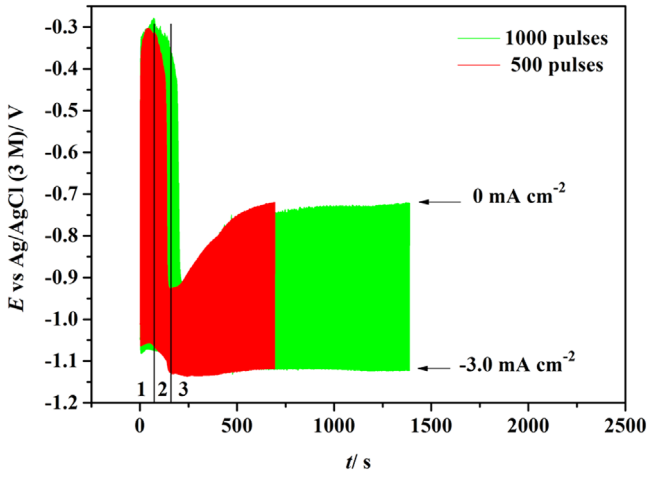

Figure 2. Potential transients obtained during pulsed electroplating. For simplicity, only the transients for the shortest and the longest procedure are presented; in addition, the regions where different features between the pulse time (T_{on}) and the relaxation time (T_{off}) were observed are identified as regions 1, 2, and 3 as detailed in the text.

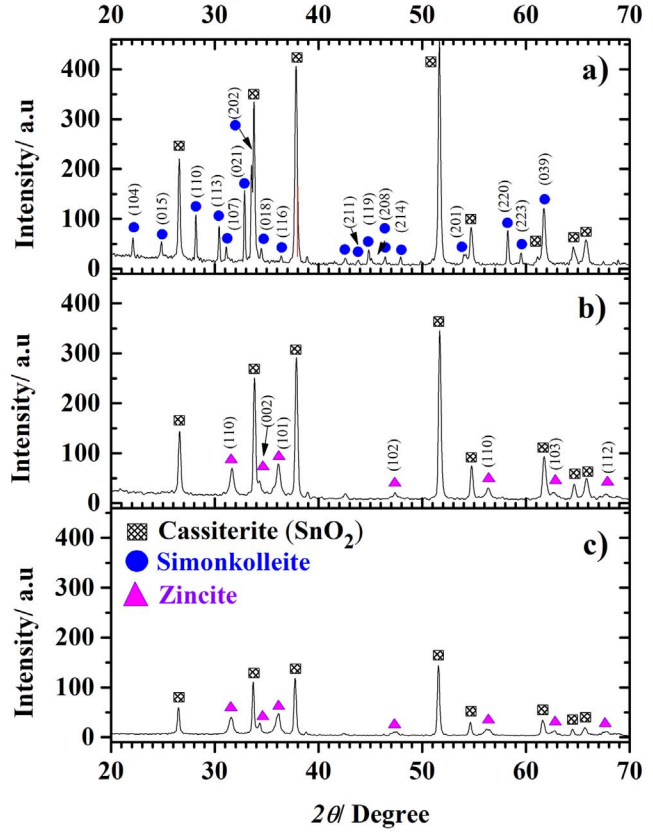

Figure 3. X-ray diffraction patterns for films obtained by pulsed electrodeposition onto FTO: (a) without any thermal treatment; (b) after a 1.5 h thermal treatment at 250 °C and 3 h immersion step in water; (c) after the 250 °C thermal treatment but without water soaking.

precipitation of Zn-containing compounds, such as $Zn(OH)_2$ (Eq. 3), which dehydrates to finally form the desired oxide (Eq. 4).

Figure 1 shows cyclic voltammograms for a $Zn(NO_3)_2{\cdot}6H_2O$ + KCl solution with prior N_2 bubbling. Starting the first scan at 0 V vs Ag/AgCl, an increase in the cathodic current is observed at potentials more negative than −1.1 V vs Ag/AgCl, which is mainly related with water reduction at the FTO surface, leading to H_2 formation (Eq. 2). Upon reversing the scan direction, a small cathodic current peak is observed at −1.02 V vs Ag/AgCl, which may be attributed to reduction of NO_3^- (Eq. 1). The observation of the anomalous cathodic peak in the reverse scan is related to the large water reduction current at more negative potentials, which results in a modification of the working electrode surface and accumulation of hydrogen evolution reaction products that may block nitrate reduction reaction at very negative potentials. Unfavorable reaction kinetics at FTO appears to be the reason of the non-appreciable cathodic current related to nitrate reduction in the first forward scan.

The activation of the FTO surface for nitrate reduction after the precipitation of a zinc-containing overlayer is indicated by the current onset shift from −1.0 to −0.67 V vs Ag/AgCl, comparing the 1st and the 2nd scan. This was confirmed by X-ray diffraction (see Supplementary Materials (available online at stacks.iop.org/JES/169/042504/mmedia)) on samples prepared by scanning the potential from 0 to −1.09 V vs Ag/AgCl (Fig. S1a), where a crystalline zinc-containing material corresponding to the mineral phase simonkolleite is observed. The presence of Cl^- in the electrodeposition solution favors the formation of simonkolleite (Eq. 5) instead of ZnO, which generally forms by dehydration of $Zn(OH)_2$.[35]

$$5\,Zn^{2+}(aq) + 8\,OH^-(aq) + 2Cl^-(aq) + H_2O\,(l) \rightarrow Zn_5(OH)_8Cl_2{\cdot}H_2O(s) \quad [5]$$

At −1.4 V vs Ag/AgCl (Fig. S1b), in addition to simonkolleite, we start to observe the presence of ZnO, and even some SnO due to the reduction of the transparent conductive oxide (TCO) substrate under these conditions of elevated temperature and neutral pH. The presence of ZnO at this potential is related to the high current density, which results in fast formation of OH^- while the incorporation of Cl^- may become partially limited by diffusion. The anodic peak observed at −0.64 V vs Ag/AgCl does not relate to the oxidation of the metallic Zn previously deposited on the electrode, as is generally observed for deposition from $ZnCl_2$ solutions.[36,37] In this case, the peak is related to two processes: the re-oxidation of SnO to SnO_2, which is accompanied by a change in color of the substrate, and a pseudo-capacitive discharging process of trapped charge in the Zn-containing layer.

To investigate the origin of the enhanced NO_3^- reduction rate on the surface-modified FTO electrode observed in the backward direction of the 1st scan, cyclic voltammetry for $NaNO_3$ and KCl solutions were carried out using FTO, ZnO and simonkolleite as working electrodes (Fig. 1b). At the FTO electrode, the current associated to NO_3^- reduction (at potentials more negative than −1.1 V vs Ag/AgCl) is low, while the cathodic current somewhat larger for the simonkolleite and ZnO electrodes. This may be partially attributed to differences in the electrode surface roughness, however, the reaction onset potential graphically calculated in the figure for ZnO and simonkolleite electrodes is clearly more positive, pointing to an increased electrocatalytic activity for nitrate reduction reaction on the zinc-containing layers. Note that the lower current densities observed in Fig. 1b compared to in Fig. 1a are due to the absence of Zn^{2+} ions in the electrolyte solution, which also play an electrocatalytic role in nitrate reduction.[31]

In order to circumvent the slow reduction reaction rate of nitrate at the FTO surface, we explored pulsed electroplating in order to deposit thicker and homogeneous films, which has positive effects on mass transport limitations, electrode kinetics and the nucleation of a larger density of growth centers, characteristics that improve the morphology and properties of deposits in addition to the film growth rate.[38] To obtain high quality and pure simonkolleite films, we evaluated deposition using 500, 600, 700 and 1000 pulses, where each pulse consists of a 0.388 s application of $-3.0\,mA\,cm^{-2}$ followed by 1 s at $0\,mA\,cm^{-2}$. At the deposition current density

Table I. Average thickness of electrodeposited simonkolleite films as function of the number of pulses: at least 5 films were prepared at each of the number of pulses shown, and the average thickness and standard deviation are provided. The variation in values for the samples prepared at 1000 pulses was larger, and these films were therefore not further used in this work.

# of pulses	Film thickness (μm)
500	4.5 ± 1
600	5.8 ± 1.4
700	5.9 ± 1.2

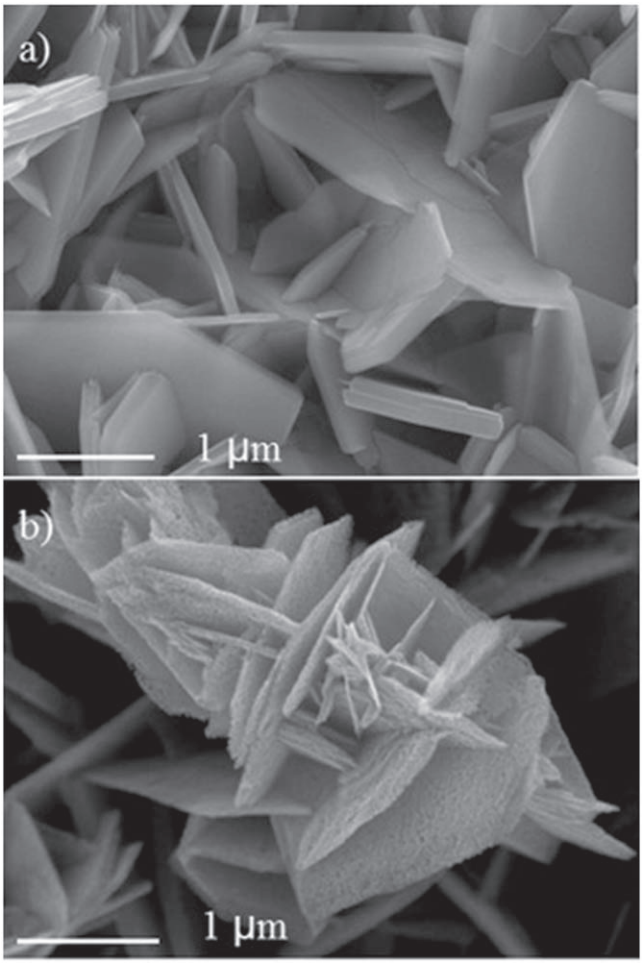

Figure 4. SEM images for films obtained by pulsed plating (700 pulses), from a 0.1 M $Zn(NO_3)_2 \cdot 6H_2O$, 0.1 M KCl aqueous solution at pH = 6.0 and 70 °C: (a) before and (b) after a 1.5 h thermal treatment at 250 °C and 3 h water immersion step.

chosen, we expect that only simonkolleite is deposited with negligible presence of ZnO.

Figure 2 shows potential transients for the pulsed deposition procedure. The potential in both the deposition (T_{on}) and the relaxation (T_{off}) step changes with time upon film growth. At the start of the procedure, in region 1 (0 − 72 s), an almost constant deposition potential of about −1.06 V vs Ag/AgCl suggests the reduction of mainly NO_3^- and some H_2O (especially in the beginning) at the electrode surface, which leads to the formation of simonkolleite crystals onto the FTO surface, as corroborated by X-ray diffraction (XRD) in Fig. 3a. When the current flow is interrupted, the potential quickly settles at −0.3 V vs Ag/AgCl as the working electrode discharges. Region 2 (72 − 160 s) is characterized by a gradual increase of the deposition potential during the plating step from −1.06 to −1.13 V vs Ag/AgCl, which is accompanied by a shift in the relaxation potential. The changes observed in region 2 suggest a modification of the working electrode surface, leading to a capacitive behavior at the substrate/solution interface as the FTO substrate is covered by the simonkolleite film. Finally, region 3 displays a shift of the relaxation potential back to less negative values. As time progresses, the film thickness increases due to the reduction reactions at the simonkolleite crystals previously grown, although the fraction of current that is capacitive increases and the Faradaic efficiency is expected to decrease, which is reflected in Table I. Note that the small differences observed between the voltage transients displayed in this figure are due to slight variations on the working area delimited and bath temperature fluctuations; however, in general, all the pulsed deposits followed the same trend.

Table I shows the average thickness of the simonkolleite deposits as a function of the number of pulses. As expected, the film thickness increases with the number of pulses, up to around 5.9 μm at 700 pulses. At longer deposition times or larger number of pulses, a lack of reproducibility was observed related to the difficulty to properly delimit the working area on the FTO substrate when immersed in an electrolyte solution at 70 °C. For this reason, for more detailed characterization and application of the films in dye-sensitized solar cells, we focus on simonkolleite films deposited using a pulse train of 700 pulses.

Previous studies on the thermal stability of simonkolleite particles have shown that several Zn compounds, including ZnO, can be obtained as function of the heat treatment temperature:[39,40]

$$110 \sim 165\ ^\circ\text{C}: \ Zn_5(OH)_8Cl_2 \cdot H_2O \rightarrow Zn_5(OH)_8Cl_2 + H_2O \quad [6]$$

$$165 \sim 210\ ^\circ\text{C}: \ Zn_5(OH)_8Cl_2 \rightarrow 2\,Zn(OH)Cl + 3\,ZnO + 3\,H_2O \quad [7]$$

$$210 \sim 300\ ^\circ\text{C}: \ 2\,Zn(OH)Cl \rightarrow ZnCl_2 + ZnO + H_2O \quad [8]$$

$$ZnCl_2 + H_2O \rightarrow ZnO + 2HCl \quad [9]$$

Based on the mechanism above, ZnO and $ZnCl_2$ (Eq. 8) are obtained upon exposure of simonkolleite films at 250 °C. Subsequent immersion in distilled water results in the dissolution of $ZnCl_2$, leaving a pure ZnO film. This is confirmed in the XRD pattern on the film after the heat treatment and water immersion step as shown in Fig. 3b. Interestingly, XRD also revealed the absence of $ZnCl_2$ even without the water immersion step (see Fig. 3c). It has been suggested that $ZnCl_2$ can react with the water vapor formed, resulting in solid ZnO and HCl in gas form, as shown in Eq. 9, which would explain our finding.[40,41] However, this hydrolysis reaction is strongly dependent on the reaction atmosphere, hence, to ensure the preparation of pure ZnO films, we maintained the water-soaking step in our preparation procedure. The diffraction peaks for the ZnO films are relatively broad (as clearly observed at 36.16° and 47.45°) indicating that the film is nanostructured.[42] The diffuse reflectance characterization and the corresponding Tauc plot for ZnO films obtained under these conditions are presented in the Supporting Information in Figs. S2a and S2b. A band gap energy (E_g) of 3.35 eV was graphically obtained from Fig. S2b using the Tauc relations and assuming a direct electronic transition with a scattering coefficient equal to 1 for ZnO, which is in good agreement with the values reported in literature.[12,20,42,43] These results highlight that crystalline ZnO with the adequate optical properties are obtained by the pulse plating of simonkolleite and subsequent thermal transformation.

The morphology of the materials before and after the treatment procedure was studied using scanning electron microscopy (SEM). As shown in Fig. 4a, the simonkolleite phase electrocrystallizes as well-defined, micron-sized hexagonal plates with low surface roughness and nonspecific orientation with respect to the substrate; in addition, no dependence was found between morphology and

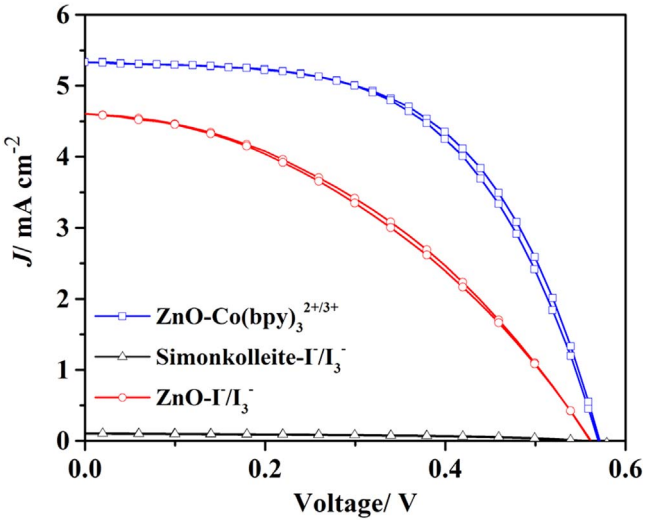

Figure 5. Current density vs voltage curves (forward and backward scan) for the best DSSCs elaborated with simonkolleite and ZnO films sensitized for 3 h in a MG-207 dye + CDCA solution at a scan rate of 50 mV s^{-1}. Two electrolyte solutions are compared, based on the $Co(bpy)_3^{2+/3+}$ and the I^-/I_3^- redox couple, respectively.

number of pulses, as shown in the supporting information in Fig. S3. After the treatment procedure, the ZnO film obtained (Fig. 4b) showed the same hexagonal plates and open structure as observed in the simonkolleite film, however, mesopores are present in the hexagonal plates due to the transformation of simonkolleite into ZnO and loss of $ZnCl_2$ and water (Eqs. 7–9). The generated mesoporous, nanostructured morphology of the hexagonal platelets leads to an increase of the surface area of the film, which is an important characteristic for application in the dye-sensitized solar cell (DSSC). The potentiostatic deposition of $ZnO/Zn_5(OH)_8Cl_2{\cdot}H_2O$ onto ITO substrates has been reported previously: films with a thickness of 3–4 μm were obtained for a 1 h deposition time, and a high temperature thermal treatment (400 °C) was used to obtain crystalline ZnO structures.[44] Hence, the procedure reported here is significantly faster and provides a low temperature route to obtain a high-quality material onto TCO substrates for photovoltaic applications.

Photovoltaic characterization of DSSCs.—Dye-sensitized solar cells were fabricated from simonkolleite films electrodeposited using a procedure of 700 pulses. The photovoltaic characteristics were evaluated both before and after the heat treatment, which consisted of thermal decomposition at 250 °C (1.5 h) and immersion in water (3 h). The recently reported benzothiadiazole dye MG-207 was used as a fully organic sensitizer,[24] and two electrolyte solutions with different redox couples have been used, comparing the traditional I^-/I_3^- redox couple with the $Co(bpy)_3^{2+/3+}$ couple.

Figure 5 shows the current density-potential curves for these solar cell devices and Table II provides the photovoltaic parameters: it can be seen that the ZnO-based cells showed much higher efficiencies than the simonkolleite-based cells, which is mainly due to much higher short circuit current densities (J_{SC}). Simonkolleite has been reported to be a semiconducting material with similar band gap as ZnO (about 3.3 eV), and has been applied in QD-sensitized solar cells recently, providing an improvement in the performance.[45] In the MG-207 sensitized solar cell based on pure simonkolleite, a well-defined current—voltage curve is obtained (see Fig. S4 in the Supplementary Materials), however, the efficiency is low. The main cause is the low amount of dye adsorbed at the film surface, which is evidenced by the very weak coloring of the simonkolleite films after sensitization. This can be explained by the small active surface area of the smooth, micron-sized simonkolleite platelets as observed in the SEM images (Fig. 4a). In addition, there may be a weak chemical interaction between the anchoring group in the dye molecule and the faces of the simonkolleite crystals, something needed to the dye physisorption.[46] Other reasons could include low electron injection efficiency from the excited state of adsorbed dye molecules into the simonkolleite conduction band due to a misalignment between energy levels, or poor collection efficiency related to fast recombination reactions at simonkolleite/electrolyte interface. Due to the low efficiency of the system, we did not further explore this, although by changing the sensitizer and electrolyte solution properties, a better efficiency may be possible.

The MG-207 sensitized ZnO-based solar cells show *J–V* curves characteristic of DSSCs, where the cells with the $Co(bpy)^{2+/3+}$ redox couple exhibit a larger short-circuit photocurrent than the cells with the I^-/I_3^- couple. It has been shown for a variety of organic dyes that regeneration of oxidized dye molecules by cobalt-based redox couples is faster than for I^-/I_3^-, even at smaller driving force given by $|E_{HOMO} - E°_{redox}|$.[47] Thus, the larger J_{SC} can be attributed to an increase of the charge injection and collection efficiency. On the other hand, the V_{OC} is very similar for the two redox couples, despite a 0.18 V difference in standard redox potential, with the $Co(bpy)^{2+/3+}$ redox couple having a more positive $E°_{redox}$.[48] These results indicate that recombination is dominated by electron transfer from the ZnO to the redox couple, and that recombination is faster for the $Co(bpy)^{2+/3+}$ couple. In recent work, we showed for a different ZnO-dye system that this is related to electrostatic interactions between the redox couple and the ZnO surface, which influences diffusion of the redox couple inside the macroporous—mesoporous film.[36] Hence, diffusion of the positively charged $Co(bpy)^{2+/3+}$ redox couple through the ZnO structures is favored over the negatively charged I^-/I_3^- couple. This has not only negative but also positive consequences, as it explains the larger fill factor observed for the $Co(bpy)^{2+/3+}$ redox couple.

In summary, the best photovoltaic performance was observed for the ZnO-$Co(bpy)^{2+/3+}$ solar cells, indicating the advantages of combining an organic dye such as MG-207 and an organometallic Co-based redox shuttle in order to obtain high-performance ZnO-based DSSCs. To our knowledge, the highest values reported for ZnO-based DSSCs are: (i) 8.0% for a plasma-treated ZnO/N-719/I^-/I_3^- system;[49] (ii) 5.9% for 1D ZnO nanowires and 4.0% for nanoparticle ZnO films for a ZnO/Ru-dye/$Co(bpy)_3^{2+/3+}$ system,[50] (iii) and up to 5.7% for 1D ZnO nanowires and 3.6% for nanoparticle ZnO films for a ZnO/Organic dye/$Co(bpy)_3^{2+/3+}$ system.[51] Although the efficiencies observed in our solar devices are somewhat lower, the system may be further improved through a detailed optimization of each component, including the ZnO film thickness, the sensitization step, ZnO surface passivation/modification, photon management, and the electrolyte composition by

Table II. Short circuit current density (J_{SC}), open circuit potential (V_{OC}), efficiency (η) and fill factor (*FF*) for the DSSCs in Fig. 5, as well as the average values and standard deviations for each photovoltaic parameter calculated for 2 cells (ZnO-I^-/I_3^-, ZnO-$Co(bpy)^{2+/3+}$) and 3 solar cells (Simonkolleite-I^-/I_3^-).

	J_{SC} (mA cm^{-2})	V_{OC} (V)	*FF*	η (%)
ZnO-I^-/I_3^-	4.60 (4.58 ± 0.04)	0.56 (0.55 ± 0.01)	0.41 (0.42 ± 0.03)	1.05 (1.06 ± 0.03)
ZnO-$Co(bpy)^{2+/3+}$	5.33 (5.22 ± 0.16)	0.58 (0.52 ± 0.08)	0.56 (0.58 ± 0.03)	1.74 (1.58 ± 0.23)
Simonkolleite- I^-/I_3^-	0.21 (0.13 ± 0.07)	0.56 (0.55 ± 0.02)	0.46 (0.48 ± 0.04)	0.053 (0.034 ± 0.17)

including specific additives. Furthermore, avoiding Ru-based dyes and the rather corrosive I^-/I_3^- electrolyte solution may provide viable opportunities for this system in lightweight, flexible photovoltaics.

Conclusions

ZnO films with a combined macroporous and mesoporous morphology were obtained by low-temperature thermal decomposition of open structures of a complex zinc hydroxychloride compound, simonkolleite, which was electrodeposited onto FTO substrates from a $Zn(NO_3)_2$/KCl solution using a pulsed plating method. For this deposition bath, the electrochemical characterization shows the expected NO_3^- reduction on the electrode surface, however, the presence of a high Cl^- concentration completely changes the material formed, leading to the electrocrystallization of hexagonal simonkolleite platelets instead of ZnO. The galvanostatic pulsed plating procedure has been designed to avoid limitations related to the slow reduction kinetics and mass transport associated with NO_3^-, resulting in the deposition of an approximately 6 μm thick film in less than 1000 s. The transformation of simonkolleite to ZnO can be achieved with a relatively low temperature thermal treatment at 250 °C, providing a nanostructured, mesoporous, crystalline ZnO film composed of micron-sized hexagonal platelets. Dye-sensitized solar cells (DSSCs) elaborated with the ZnO films described above showed an encouraging power conversion efficiency of 1.7% for the combination of the organic benzothiadiazole dye MG-207 and an electrolyte solution based on the $Co(bpy)_3^{2+/3+}$ redox couple, which is expected to improve with further optimization. The fast deposition of thick simonkolleite films and its low temperature transformation into ZnO holds promise for the fabrication of portable and lightweight photovoltaic devices.

Acknowledgments

The authors gratefully acknowledge funding from CONACYT Mexico under Basic Sciences grant CB-A1-S-21018, Frontier Science grant FORDECYT-PRONACES/848260/2020, AMEXCID SRE-Conacyt-2016–1 grant 278320, and the Ministerio de Ciencia e Innovación of Spain, Agencia Estatal de Investigación (AEI) and EU (FEDER) under grant PID2019–110430GB-C22. Support from the Ministerio de Universidades and Universidad Pablo de Olavide through the Beatriz Galindo program under project BEAGAL 18/00077 and grant BGP 18/00060 is also acknowledged. R.D. and J.M. A.C. acknowledge the European Research Council (ERC) for funding. This work was partially funded under the European Union's Horizon 2020 research and innovation program (grant agreement number 832606; project PISCO). R.D. acknowledges Dr. M. Godfroy for having developed the first synthesis of MG-207 dye.

ORCID

Renaud Demadrille https://orcid.org/0000-0002-7455-5709
Gerko Oskam https://orcid.org/0000-0002-2105-5874

References

1. M. Schlesinger and M. Paunovic, *Modern Electroplating* (New York)(Wiley) (2010).
2. A. A. Ojo and I. M. Dharmadasa, *Coatings*, **8**, 262 (2018).
3. H. H. Lou and Y. Huang, *Encycl. Chem. Process.*, **1**, 839 (1978).
4. I. M. Dharmadasa and J. Haigh, *J. Electrochem. Soc.*, **153**, G47 (2006).
5. S. A. Patil, D. V. Shinde, D. Young-Ahn, D. V. Patil, K. K. Tehare, V. V. Jadhav, J. K. Lee, R. S. Mane, N. K. Shresthaa, and S. H. Han, *J. Mater. Chem. A*, **2**, 13519 (2014).
6. H. C. Lim, E. Park, I. S. Shin, and J. I. Hong, *Bull. Korean Chem. Soc.*, **41**, 358 (2020).
7. D. C. Madu, S. M. Islam, H. Pan, and C. J. Barile, *J. Mater. Chem. C*, **9**, 6297 (2021).
8. D. Lincot, *Thin Solid Films*, **487**, 40 (2005).
9. C. Cavallo, F. Di Pascasio, A. Latini, M. Bonomo, and D. Dini, *J. Nanomater.*, **2017**, 1 (2017).
10. J. A. Anta, E. Guillén, and R. Tena-Zaera, *J. Phys. Chem. C*, **116**, 11413 (2012).
11. Q. Zhang, C. S. Dandeneau, X. Zhou, and G. Cao, *Adv. Mater.*, **21**, 4087 (2009).
12. A. B. Djurišić, A. M. C. Ng, and X. Y. Chen, *Prog. Quantum Electron.*, **34**, 191 (2010).
13. A. Kathalingam, M. R. Kim, Y. S. Chae, and J. K. Rhee, *J. Korean Phys. Soc.*, **55**, 2476 (2009).
14. L. Zhang, Z. Chen, Y. Tang, and Z. Jia, *Thin Solid Films*, **492**, 24 (2005).
15. H. Muguerra, G. Berthoux, W. Z. N. Yahya, Y. Kervella, V. Ivanova, J. Bouclé, and R. Demadrille, *Phys. Chem. Chem. Phys.*, **16**, 7472 (2014).
16. N. K. Shrestha, K. Lee, R. Hahn, and P. Schmuki, *Electrochem. Commun.*, **34**, 9 (2013).
17. N. S. Lewis, *Science*, **315**, 798 (2007).
18. A. Hagfeldt, G. Boschloo, L. Sun, L. Kloo, and H. Pettersson, *Chem. Rev.*, **110**, 6595 (2010).
19. J. Gong, J. Liang, and K. Sumathy, *Renew. Sustain. Energy Rev.*, **16**, 5848 (2012).
20. V. Thavasi, V. Renugopalakrishnan, R. Jose, and S. Ramakrishna, *Mater. Sci. Eng. R*, **63**, 81 (2009).
21. B. O'Regan and M. Grätzel, *Nature*, **353**, 737 (1991).
22. G. Li, L. Sheng, T. Li, J. Hu, P. Li, and K. Wang, *Sol. Energy*, **177**, 80 (2019).
23. S. S. Kim, J. H. Yum, and Y. E. Sung, *J. Photochem. Photobiol. A Chem.*, **171**, 269 (2005).
24. F. Bittner, T. Oekermann, and M. Wark, *Materials (Basel).*, **11**, 232 (2018).
25. F. I. Lizama-Tzec, M. A. Aguilar-Frutis, G. Rodríguez-Gattorno, and G. Oskam, *J. New Mater. Electrochem. Syst.*, **215**, 209 (2013).
26. S. Sheehan, P. K. Surolia, O. Byrne, S. Garner, P. Cimo, X. Li, D. P. Dowling, and K. R. Thampi, *Sol. Energy Mater. Sol. Cells*, **132**, 237 (2015).
27. K. Namsheer and C. S. Rout, *RSC Adv.*, **11**, 5659 (2021).
28. M. Godfroy et al., *Sustain. Energy Fuels*, **5**, 144 (2021).
29. T. Yoshida et al., *Adv. Funct. Mater.*, **19**, 17 (2009).
30. T. Yoshida and H. Minoura, *Adv. Mater.*, **12**, 1219 (2000).
31. T. Yoshida, D. Komatsu, N. Shimokawa, and H. Minoura, *Thin Solid Films*, **451–452**, 166 (2004).
32. X. Gan, X. Gao, J. Qiu, and X. Li, *Appl. Surf. Sci.*, **254**, 3839 (2008).
33. Z. Chen, Y. Tang, L. Zhang, and L. Luo, *Electrochim. Acta*, **51**, 5870 (2006).
34. F. Hu, Y. Xia, Z. Guan, X. Yin, and T. He, *Electrochim. Acta*, **69**, 97 (2012).
35. M. R. Mahmoudian, W. J. Basirun, Y. Alias, and M. Ebadi, *Appl. Surf. Sci.*, **257**, 10539 (2011).
36. E. J. Canto-Aguilar, M. Rodríguez-Perez, R. García-Rodríguez, F. I. Lizama-Tzec, A. T. De Denko, F. E. Osterloh, and G. Oskam, *Electrochim. Acta*, **258**, 396 (2017).
37. B. Canava and D. Lincot, *J. Appl. Electrochem.*, **30**, 711 (2000).
38. M. Rudolph, T. Loewenstein, E. Arndt, Y. Zimmermann, A. Neudeck, and D. Schlettwein, *Phys. Chem. Chem. Phys.*, **11**, 3313 (2009).
39. O. Garcia-Martinez, E. Vila, J. L. Martin de Vidales, R. M. Rojas, and K. Petrov, *J. Mater. Sci.*, **29**, 5429 (1994).
40. I. Rasines and J. I. M. De Setien, *Thermochim. Acta*, **37**, 239 (1980).
41. O. K. Srivastava and E. A. Secco, *Can. J. Chem.*, **45**, 1375 (1967).
42. S. Talam, S. R. Karumuri, and N. Gunnam, *ISRN Nanotechnol.*, **2012**, 1 (2012).
43. A. Janotti and C. G. Van de Walle, *Reports Prog. Phys.*, **72**, 126501 (2009).
44. J. Qiu, M. Guo, and X. Wang, *ACS Appl. Mater. Interfaces*, **3**, 2358 (2011).
45. H. Chen, L. Zhu, H. Liu, and W. Li, *Electrochim. Acta*, **105**, 289 (2013).
46. F. I. Lizama-Tzec, R. García-Rodríguez, G. Rodríguez-Gattorno, E. J. Canto-Aguilar, A. G. Vega-Poot, B. E. Heredia-Cervera, J. Villanueva-Cab, N. Morales-Flores, U. Pal, and G. Oskam, *RSC Adv.*, **6**, 37424 (2016).
47. S. M. Feldt, G. Wang, G. Boschloo, and A. Hagfeldt, *J. Phys. Chem. C*, **115**, 21500 (2011).
48. S. M. Feldt, E. A. Gibson, E. Gabrielsson, L. Sun, G. Boschloo, and A. Hagfeldt, *J. Am. Chem. Soc.*, **132**, 16714 (2010).
49. Y. He, J. Hu, and Y. Xie, *Chem. Commun.*, **51**, 16229 (2015).
50. D. Barpuzary, A. S. Patra, J. V. Vaghasiya, B. G. Solanki, S. S. Soni, and M. Qureshi, *ACS Appl. Mater. Interfaces*, **6**, 12629 (2014).
51. D. Barpuzary, A. Banik, A. N. Panda, and M. Qureshi, *J. Phys. Chem. C*, **119**, 3892 (2015).